Stretching Operational Life of Trickle-Bed Filters by Liquid-Induced Pulse Flow

Ion Iliuta and Faïçal Larachi
Chemical Engineering Department, Laval University, Québec G1K 7P4 Canada

DOI 10.1002/aic.10470
Published online May 9, 2005 in Wiley InterScience (www.interscience.wiley.com).

When dilute liquid suspensions contaminated with fine solids are treated in catalytic trickle-bed reactors, bed plugging develops and increases the resistance to two-phase flow until ultimate unit shutdown for bed substitution with pristine catalyst. The release of deposited fines, or the inhibition of fines deposition over some regions of the collector, is expected to alleviate the plugging if liquid flow shock or periodic operation policies are implemented. Current physical models linking gas–liquid phase flow to space–time evolution of fines deposition and release are unable to depict this new type of filtration in trickle beds. This work attempts to fill in this gap by developing a dynamic multiphase flow deep-bed filtration model. The model incorporates the physical effects of porosity and effective specific surface area changes as a result of fines deposition/release, gas and suspension inertial effects, and coupling effects between the filtration parameters and the interfacial momentum exchange force terms. The release of the fine particles from the collector surface was assumed to be induced by the colloidal forces in the case of Brownian particles or by the hydrodynamic forces in the case of non-Brownian particles. An important finding of the work was that for noncolloidal fines both induced pulsing and liquid flow shock operations conferred substantial improvements (measured in terms of reduction in specific deposit and pressure drop) in the mitigation of plugging in trickle-bed reactors. However, because of the highest critical shear stress for fines in the colloidal range, induced pulsing did not substantiate any practically useful effect. © 2005 American Institute of Chemical Engineers *AIChE J,* 51: 2034–2047, 2005
Keywords: trickle beds, two-phase flow, plugging, particle deposition/release, induced pulsing

Introduction

One of the major unsolved complex problems confronting the chemical and petroleum industries at present is the *deposition* of fine particles dissolved or suspended in fluid flow systems.[1-4] When heavy gas oil suspensions containing a low concentration of *nonfilterable* fine solid impurities are treated in trickle-bed hydrotreaters, plugging develops and leads to the progressive obstruction of the bed that is accompanied with an increase in pressure drop. Although the concentration of fine particles is in the range of 100 weight ppm, the cumulative effect of several months of refining operation diverts the catalyst bed from its *catalytic* function to that of a huge filter where accumulation of fines causes the pressure to rise by restricting the flow. In these conditions the unit must often be shut down to unload the *physically deactivated* catalyst for replacement with a pristine one.

Studies of fine particle deposition in packed beds experiencing nonionic liquid flows tend to support the contention that plugging with petroleum-like suspensions occurs by a deep-bed filtration mechanism,[1,5] which has its roots in the vast realm of water treatment and purification. Despite the important efforts invested over several decades to understand its underlying phenomena, deep-bed filtration remains a actively researched

Correspondence concerning this article should be addressed to F. Larachi at faical.larachi@gch.ulaval.ca.

topic. Intermingling between the hydrodynamics, the fine–collector and fine–fine surface interactions, and the physicochemical mechanisms developing inside the porous bed makes the process fundamentals difficult to grasp. Numerous investigators in the past have attempted to describe the transient behavior of deep-bed filtration, at the macroscopic and microscopic level, in the case of single-phase flow through porous media.[6-22] The macroscopic studies are aimed at the phenomenological description of deep-bed filtration process, the prediction of its dynamic behavior, and the development of methodology and techniques for design, calculation, and optimization. Microscopic theories in deep-bed filtration are intended to provide information and insight about the mechanisms of particle deposition, the conditions under which deposition may be facilitated, and the effect of deposition on the structure of packed bed media. In contrast, the literature still remains scanty concerning the complex hydrodynamics and surface phenomena involved in the plugging with fine particles of packed bed gas–liquid–solid reactors despite the critical operational problem of fines in the petroleum refining industry. Thus, a limited number of experimental works on the process of fines accumulation[2,5,23,24] and only some attempts concerning the modeling and conceptualization of dynamics of fines deposition have been reported.[3,4,25,26] The few available experimental studies showed that the pressure drop increases monotonically with the concentration of fine particles and this increase correlates well with the reduction in effective porosity arising from the accumulation of the fines. All the experimental studies suggest that the major change resulting from deposition of fine particles involves the effective size and geometry of catalyst particles, the surface characteristics of the catalyst particles, the porosity, and the effective porosity of the bed.

One of the important aspects during plugging with fine particles is the *release* of fine particles from pore bodies within the porous bed arising from the hydrodynamic or colloidal forces. It has been observed that the release of fines is a threshold process, that is, a minimum perturbation is required to detach the fines from the pore surface.[27] This could be in terms of a critical hydrodynamic stress[28] or a critical salt concentration.[29] The released fine particles, while flowing with the liquid phase, can either re-adhere to the collector surface, flow without capture, or get entrapped at the pore constrictions. A limited number of experimental works on the detachment of fine particles[30-34] and only some attempts concerning the modeling and conceptualization of the detachment dynamics of fine particles[32,33,35-37] have been reported.

Currently, physical models linking gas–liquid flow to the filtration process in trickle beds neglected the possible *release* of fine particles[3,4,25,26] and the potential beneficial impact of induced pulsing to reduce the plugging in trickle beds. An attempt has therefore been made in this work in which the authors sought to develop a dynamic multiphase flow model based on the volume average mass, momentum, and species balance equations. Coupling between the liquid suspension and solids was monitored by the fines filtration rate equation, the fines release rate equations, and the interaction drag or momentum exchange force terms. Monolayer and multiple-layer deposition mechanisms are accounted for by including the appropriate filter coefficient expressions.[38] The release of the fine particles from the collector surface was supposed to be induced by the colloidal forces in the case of Brownian particles or by the hydrodynamic forces in the case of non-Brownian particles. The incidence of fines buildup is evaluated in terms of pressure drop rise as a function of time, as well as in terms of plugging patterns for the local porosity and the specific deposit vs. bed depth. The effect of periodic operation of trickle-bed reactor on the release of fine particles was studied more specifically as a possible novel strategy for stretching the life cycle of trickle-bed hydrotreaters with the long-term objective of preventing accumulation of fines.

Governing Equations for Deposition and Detachment of Fine Particles in Trickle-Bed Reactors

A cocurrent two-phase trickle flow through a porous medium of uniform initial porosity ε^0 and single-sized catalytic particles is considered. For each flowing phase, we shall assume unidirectional, isothermal, incompressible, viscous Newtonian, and passive (no chemical reaction) conditions. The gas/liquid/fine/porous medium multiphase system is viewed as a system of three interpenetrated continua: (1) a flowing gas phase; (2) a dilute *pseudo-homogeneous* suspension phase consisting of the liquid and the seeding fine particles, hereafter referred to as *fluid*; (3) and a stationary *pseudo-continuous* solid phase made up of the packing particles—also referred to as *collectors* in this work—constituting the clean porous medium as well as of the fine particles that get captured onto their surface.

Further assumptions inherent to the formulation developed here are:

- The fluid properties, such as density, viscosity, and holdup, are equal to those of the embracing liquid (volume fraction of inlet fine particles usually down to 0.1‰).
- The bed is partially wetted by the liquid phase.
- Two-phase flow is annular and completely separated.
- Each phase, that is, gas, liquid, and solid, behaves as a continuum so that the macroscopic differential balance equations can be applied; however, except the solid mass conservation, the solid stress balance is not included in the present analysis.
- Variations of concentration of fine particles and other quantities are significant only in the major flow direction, that is, axial direction here.
- The coupling between the fluid and solid phases is monitored by the fines filter rate equation and the interfacial drag forces.
- Only the inlet liquid was considered as a source for fines without considering fines generated in the catalyst bed (resulting from attrition, byproduct buildup, and so on).
- The fine particles seeded in the liquid are considered single-sized with density ρ_f and diameter d_f.
- Bed plugging by the blocking and the sieving modes does not occur.[14,39]
- The filtration mechanism to occur is of the deep-bed filtration type and not of the cake-filtration type[1,5]; in other words fine–fine attractive interactions within the fluid phase are assumed absent or at least small enough to preclude flocculation.
- The gas–liquid interface is impervious to the fine particles. Migration of fines to the gas–liquid interface caused by fine surface properties, akin to froth flotation in mineral processing, have been neglected in the present analysis. The importance of

such migration of fines in trickle-bed flows is still to be elucidated as well as the criteria to be used to identify whether it is important.

- Another issue relates to size and wettability (or contact angle) of fines that may have an importance and that has also been neglected in the present development.
- The net sink in the fluid momentum balance resulting from the mass transfer of fine particles from the fluid to the collector is negligibly small.
- In the case of colloidal (Brownian) particles ($d_f < 2\ \mu$m), the release of fine particles from the collector surface is controlled by the colloidal forces (Brownian diffusion through the hydrodynamic boundary layer in the absence of energy barrier).[34,27]
- In the case of non-Brownian particles the release or detachment of fine particles is induced by hydrodynamic forces.[27]

The model is based on the volume-average form of the transport equation developed for multiphase systems.[40] The general model equations consist of the conservation of volume, the continuity and the Navier–Stokes equations for the gas and the fluid phases, the continuity equation for the solid stationary phase, and the species balance equation for the fines undergoing migration from the fluid phase to the solid phase:

Conservation of Volume

$$\varepsilon_g + \varepsilon_l = \varepsilon \tag{1}$$

Continuity Equations for Gas, Fluid, and Solid Phases

$$\frac{\partial}{\partial t}(\varepsilon_g \rho_g) + \frac{\partial}{\partial z}(\varepsilon_g \rho_g u_g) = 0 \tag{2}$$

$$\frac{\partial}{\partial t}(\varepsilon_l \rho_l) + \frac{\partial}{\partial z}(\varepsilon_l \rho_l u_l) = -\gamma \rho_f N + (1-\gamma)\rho_f r^h_{\text{det}} + \rho_f r^c_{\text{det}} \tag{3}$$

$$\frac{\partial}{\partial t}[(1-\varepsilon^0)\rho_s + (1-\varepsilon_d)(\varepsilon^0 - \varepsilon)\rho_f] = \gamma \rho_f N - (1-\gamma)\rho_f r^h_{\text{det}} - \rho_f r^c_{\text{det}} \tag{4}$$

Species Balance Equation for Fines

$$\frac{\partial}{\partial t}(\varepsilon_l c) + u_l \frac{\partial}{\partial z}(\varepsilon_l c) = -\gamma N + (1-\gamma) r^h_{\text{det}} + r^c_{\text{det}} + D_l \frac{\partial^2}{\partial z^2}(\varepsilon_l c) \tag{5}$$

Momentum Balance Equations for Dispersed Gas and Continuous Fluid Phases

$$\frac{\partial}{\partial t}(\rho_g \varepsilon_g u_g) + u_g \frac{\partial}{\partial z}(\rho_g \varepsilon_g u_g) = \varepsilon_g \mu^e_g \frac{\partial^2 u_g}{\partial z^2} - \varepsilon_g \frac{\partial P}{\partial z} + \varepsilon_g \rho_g g - F_{gl} - F_{gs} \tag{6}$$

$$\frac{\partial}{\partial t}(\rho_l \varepsilon_l u_l) + u_l \frac{\partial}{\partial z}(\rho_l \varepsilon_l u_l) = \varepsilon_l \mu^e_l \frac{\partial^2 u_l}{\partial z^2} - \varepsilon_l \frac{\partial P}{\partial z} + \varepsilon_l \rho_l g + \frac{\varepsilon \eta_e - \varepsilon_l}{\varepsilon_g}[F_{gl} + F_{gs}] - F_{ls} \tag{7}$$

It should be noted that in the case of non-Brownian fine particles, in the previous general model, the rate of colloidal particle entrainment is negligible (r^c_{det}). On the other hand, in the case of Brownian particles the rate of hydrodynamic particle entrainment is negligible (r^h_{det}).

In the preceding model, P stands for pressure; ε_α, ρ_α, and u_α represent, respectively, the holdup, the density, and the longitudinal (interstitial) velocity of phase α (gas or fluid phases), whereas the subscripts s and f refer to the solid phase (or collectors) and fines, respectively. $F_{\alpha-\beta}$ represents the interfacial drag force per unit reactor volume exerted at the interface between mutually interacting α and β phases (gas, fluid, and solid phases). The fluid-phase effective viscosity μ^e_α, which arises from the combination of the viscous and the pseudo-turbulence stress tensors, is formulated as proposed by Dankworth et al.[41] In addition, g is the acceleration attributed to gravity, ε is the local porosity at time t, ε^0 is the initial *clean* bed porosity, ε_d is the porosity of fine particles deposit, c is the local fines volumetric concentration, N is the local filtration rate, and γ represents the fraction of the collector surface area available for adhesion of fine particles. Note that in the formulation of the momentum balance equations, the capillary pressure between liquid and gas phases is neglected.

The fine particles are imposed in the influent stream as a fluid step-increase function after suddenly switching from steady-state flow of clean or *fines-free* gas–liquid flow through the immaculate porous medium. Solution of this initial state is obtained by solving for $c = 0$, $N = 0$, $r^h_{\text{det}} = 0$, and $r^c_{\text{det}} = 0$ the conservation of volume, the continuity, and the momentum balance equations for the gas and the unloaded liquid, as follows

$$\varepsilon^0_g + \varepsilon^0_l = \varepsilon^0 \tag{8}$$

$$\frac{\partial}{\partial t}\varepsilon^0_g \rho^0_g + \frac{\partial}{\partial z}\varepsilon^0_g \rho^0_g u^0_g = 0 \tag{9}$$

$$\frac{\partial}{\partial t}\varepsilon^0_l \rho_l + \frac{\partial}{\partial z}\varepsilon^0_l \rho_l u^0_l = 0 \tag{10}$$

$$\frac{\partial}{\partial t}(\rho^0_g \varepsilon^0_g u^0_g) + u^0_g \frac{\partial}{\partial z}(\varepsilon^0_g \rho^0_g u^0_g) = \varepsilon^0_g \mu^{e0}_g \frac{\partial^2 u^0_g}{\partial z^2} - \varepsilon^0_g \frac{\partial P}{\partial z} + \varepsilon^0_g \rho^0_g g - F^0_{gl} - F^0_{gs} \tag{11}$$

$$\frac{\partial}{\partial t}(\rho_l \varepsilon^0_l u^0_l) + u^0_l \frac{\partial}{\partial z}(\varepsilon^0_l \rho_l u^0_l) = \varepsilon^0_l \mu^{e0}_l \frac{\partial^2 u^0_l}{\partial z^2} - \varepsilon^0_l \frac{\partial P}{\partial z} + \varepsilon^0_l \rho_l g + \frac{\varepsilon^0 \eta_e - \varepsilon^0_l}{\varepsilon^0_g}[F^0_{gl} + F^0_{gs}] - F^0_{ls} \tag{12}$$

where the superscript 0 stands for the clean (initial) bed flow state.

The problem depicted by the preceding conservation equations (Eqs. 1–7) is $1 - D + t$, which contains seven unknowns: ε_l, ε_g, ε, u_l, u_g, P, and c. It further contains seven dependent unknowns: the filtration rate N; the fraction of the collector surface area available for the adhesion of fine particles γ; the release rates of fine particles r^h_{det} and r^c_{det}; and the interfacial gas–liquid, gas–solid, and liquid–solid drag forces, F_{gl}, F_{gs}, and F_{ls}, which require additional closure formulations.

Filtration rate model

The filtration (or deposition) rate determines the degree of collection of fines. The filtration rate is related to the specific deposit σ, which represents the volume of fines deposited per unit reactor volume.[38]

$$\frac{d\sigma}{dt} = N\gamma - r^h_{\text{det}}(1-\gamma) - r^c_{\text{det}} \tag{13}$$

The logarithmic law of Iwasaki[42] was used to express the dependency of the deposition rate on the concentration of fine particles and the superficial liquid velocity

$$N = \lambda c v_l \tag{14}$$

In Eq. 14, λ is the filter coefficient that can be thought of as the probability for a fine to be captured as it travels a unit distance through the bed.[38] The form of the filter coefficient is dictated by both the nature of the capture phenomena in play and the amount of capture as bed plugging proceeds.

- For $\sigma \le \sigma_{cr}$ (initial stage: fines adhere individually as a monolayer on the collector surface)

$$\lambda = \lambda^0 = \frac{3}{2}(1-\varepsilon^0)^{1/3}\frac{\eta^0}{d^0_p} \qquad \text{(sphere-in-cell model[11])} \tag{15}$$

where

$$\eta^0 = \frac{3}{2}A^0_s(1-\varepsilon^0)^{2/3}N^2_R\left[\frac{2}{3}N^{1/8}_L N^{-1/8}_R + \frac{9}{4000}N^{6/5}_G N^{-12/5}_R\right] + 4(A^0_s)^{1/3}(1-\varepsilon^0)^{2/3}N^{-2/3}_{Pe} \tag{16}$$

$$A^0_s = \frac{2(1-p^5)}{w} \qquad p = (1-\varepsilon^0)^{1/3}$$
$$w = 2 - 3p + 3p^5 - 2p^6 \tag{17}$$

- For $\sigma > \sigma_{cr}$ (multilayer deposition[43])

$$\frac{\lambda}{\lambda^0} = B_1\frac{A_s}{A^0_s}\left[1 + \frac{\sigma}{(1-\varepsilon^0)(1-\varepsilon_d)}\right]^{17/24} + B_2\frac{A_s}{A^0_s}\left[1 + \frac{\sigma}{(1-\varepsilon^0)(1-\varepsilon_d)}\right]^{4.4/3} + B_3\left(\frac{A_s}{A^0_s}\right)^{1/3}\left[1 + \frac{\sigma}{(1-\varepsilon^0)(1-\varepsilon_d)}\right]^{4/9} \tag{18}$$

where

$$B_1 = \frac{(1-\varepsilon^0)^{2/3}}{\eta^0}A^0_s N^{1/8}_L N^{15/8}_R \tag{19}$$

$$B_2 = 3.376\times 10^{-3}\frac{(1-\varepsilon^0)^{2/3}}{\eta^0}A^0_s N^{1.2}_G N^{-0.4}_R \tag{20}$$

$$B_3 = \frac{4\sqrt[3]{A^0_s}\,N^{-2/3}_{Pe}}{\eta^0} \tag{21}$$

$$\frac{A_s}{A^0_s} = \left[\frac{1-(1-\varepsilon)^{5/3}}{1-(1-\varepsilon^0)^{5/3}}\right] \times \left[\frac{2-3(1-\varepsilon^0)^{1/3}+3(1-\varepsilon^0)^{5/3}-2(1-\varepsilon^0)^2}{2-3(1-\varepsilon)^{1/3}+3(1-\varepsilon)^{5/3}-2(1-\varepsilon)^2}\right] \tag{22}$$

The critical specific deposit σ_{cr} corresponds to the amount of fines required for completing a monolayer having a coating porosity ε_d. σ_{cr} is calculated assuming the sphere-in-cell model configuration[19]

$$\sigma_{cr} = \left[\left(\frac{d^0_p + 2d_f}{d^0_p}\right)^3 - 1\right](1-\varepsilon_d)(1-\varepsilon^0) \tag{23}$$

Release rate of fine particles

For non-Brownian fine particles, the rate of hydrodynamic particle entrainment was considered to be proportional to the difference between the wall shear stress and the critical shear stress[27,28]

$$r^h_{\text{det}} = \alpha^h_{\text{det}}\bar{a}(1-\varepsilon)\eta_e(\tau_w - \tau_{cr})\frac{1}{\rho_f} \qquad \text{for } \tau_w > \tau_{cr} \tag{24}$$

$$r^h_{\text{det}} = 0 \qquad \text{for } \tau_w < \tau_{cr} \tag{25}$$

Physically, Eqs. 24 and 25 indicate that to initiate the fine particles release, the wall shear stress as a result of liquid (and indirectly gas) flows should be greater than a *critical shear stress*. Implicit in this formulation is the assumption that the critical shear stress is an indicator of the strength of intraparticle bonds binding the fine particles to the pore wall. In the case of Brownian particles, the release by hydrodynamic mechanism is not possible because of the much higher values of critical shear stress required for detachment.

For colloidally induced release (Brownian fine particles), in the absence of an energy barrier, the rate of particle detachment is based on the assumption that the rate-limiting step is the

diffusion of detached colloids across the boundary layer between collector surfaces and the liquid bulk[34]

$$r^c_{\text{det}} = \alpha^c_{\text{det}} \bar{a}(1 - \varepsilon)\eta_e d_f \sigma \tag{26}$$

where α^c_{det} is the first-order release rate coefficient, reflecting diffusive transport of detached colloids across the diffusion boundary layer, that depends on the colloid diffusion coefficient and the boundary layer thickness[34]

$$\alpha^c_{\text{det}} = \frac{D_{\text{BM}}}{\delta^2_{bl}} \tag{27}$$

It is worth noting that an added complexity, not considered in the development of the present model but is actually observed in actual filtration laboratory experiments, is the release of flocs of aggregated fines stemming from shear forces rather than individual particles. Setbacks potentially brought about by such flocs during their migration and reattachment downstream of the bed could even worsen the pressure drop increase as a result of severe localized spots of plugging. These floc phenomea are not included in the present model.

One additional remark worth mentioning concerns the insufficient knowledge to quantify particle entrainment in nonconsolidated porous media such as trickle-bed reactors. As a matter of fact, results reported in the majority of the extant literature concern consolidated porous media.[34,35] However, according to the findings of Sen et al.,[37] it is still possible to characterize transport of fines in nonconsolidated porous media having porosity near 30%. This porosity constitutes a realistic lower limit threshold for nonconsolidated porous media such as those dealt with in this work.

Critical shear stress–hydrodynamic particle release

The retention of fine particles in a fixed bed requires that the adhesion force between a retained fine particle and a collector is at least in equilibrium with the hydrodynamic force, which tends to detach the fine particle.[32] Particle detachment thus occurs only when the hydrodynamic force overcomes this adhesive force. Three potential particle-removal mechanisms are known to occur: lifting, sliding, and rolling.[32,44] As rolling particle can occur over a collector surface and does not necessarily lead to particle detachment and, because in the case of non-Brownian particles the lifting force is much lower that the maximum adhesion force,[44] the following analysis is therefore based on the sliding mechanism.[32]

The main forces acting on the fine particles include the adhesion forces, responsible for fine particle attachment, and the hydrodynamic forces, responsible for fine particle release (Figure 1). The adhesion forces are those of the London–van der Waals force, which acts in the direction normal to the collector plane and is always attractive (F_V) and the electrical double layer force that acts in the direction normal to the collector plan and is usually repulsive (F_E). The hydrodynamic forces are: the drag force experienced by the fine particle resulting from the fluid flow in the tangential direction along the collector plan (F_D); the lifting force that is in the direction normal to the collector plan (F_L); and the friction force against particle sliding (F_F).

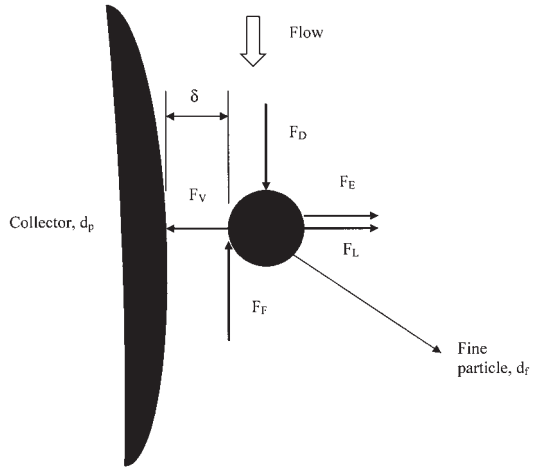

Figure 1. Forces acting on a spherical fine particle attached to a collector plan with a stagnant film of liquid on the surface.

To calculate the critical shear stress, the extreme case where the attached particles experience only attractive force is considered. This situation applies to attached particles in close contact with the collector. Thus, by neglecting the effect of F_E, the maximum adhesion force is

$$F_{A,\max} \cong F_V \tag{28}$$

The total van der Waals force for a smooth, deformable particle adhering to a smooth surface is

$$F_V = \frac{\text{Ha}\, d_f^3}{12\delta^2(\delta + d_f)^2} \cong \frac{\text{Ha}\, d_f}{12\delta^2} \tag{29}$$

where δ is the separation distance between the fine particle and the collector plane ($\delta = 1.65 \times 10^{-10}$ m).[45]

The hydrodynamic force on a spherical particle of diameter d_f in contact with a planar wall in a slow linear shear flow has been calculated by Goldman et al.[46] and can be directly related to the local wall shear stress

$$F_D = 2.551\,\pi d_f^2 \tau \tag{30}$$

The shear stress acting on the collector was estimated using Happel's model

$$\tau = 3\mu_l \frac{A_s}{d_p} u_l \tag{31}$$

where

$$A_s = \frac{2(1 - p^5)}{w} \qquad p = (1 - \varepsilon)^{1/3}$$

$$w = 2 - 3p + 3p^5 - 2p^6 \tag{32}$$

The friction force against the sliding particle may be assumed to be proportional to the adhesive force[32]

$$F_F = k_F \frac{6(1-\varepsilon^0)}{d_p^0} F_{A,\max} = k_f \frac{6(1-\varepsilon^0)}{d_p^0} \frac{\mathrm{Ha}\, d_f}{12\delta^2} \quad (33)$$

By using Eqs. 30 and 33, the net force acting on an attached particle in a deep-bed filter along the tangential direction is given by

$$F = F_F - F_D = k_f \frac{6(1-\varepsilon^0)}{d_p^0} \frac{\mathrm{Ha}\, d_f}{12\delta^2} - 2.551\pi d_f^2 \tau \quad (34)$$

When the net force $F \geq 0$ there is no particle detachment and when $F < 0$ there is a sliding of the deposited particle and subsequently its detachment. For the condition of equilibrium between the friction and drag forces we can estimate the critical shear stress as

$$\tau_{cr} = \frac{k_f \dfrac{6(1-\varepsilon^0)}{d_p^0} \dfrac{\mathrm{Ha}}{12\delta^2}}{2.551\pi d_f} \quad (35)$$

Interfacial drag forces

The assumption of bed partial wetting entrains that the gas-phase drag will have contributions because of effects located at the gas–liquid (F_{gl}) and gas–solid (F_{gs}) interfaces. Similarly, the resultant of the forces exerted on the liquid phase involves two components: (1) the drag force (F_{ls}), experienced by the liquid as a result of the shear stress near the liquid–solid boundary; and (2) the gas–liquid interfacial drag arising from the slip between fluids (F_{gl}).

Under trickle flow conditions, the double-slit flow analogy yields a satisfactory approximation of the constitutive equations needed for the gas–liquid, liquid–solid, and gas–solid drag forces.[47]The double-slit flow becomes well representative of the gas-continuous flow regimes when the liquid texture is mainly contributed by packing-supported liquid films and rivulets, and the gas–liquid separated flow and gas flow assumption holds. This generally occurs at low liquid flow rates that allow the transport of liquid in the form of a smooth and stable film.[48] Because the actual trickle-flow structure, which is conceptualized by a simplified cell of two parallel interconnected inclined slits [a gas–liquid slit corresponding to the region $a_s\eta_e$, and a dry slit corresponding to the region $a_s(1-\eta_e)$], the force balance equations for the gas and liquid are first solved in the slit scale and are then mapped into the bed scale. At a given depth z in the bed, the projections of the drag forces take the following forms[49]:

$$F_{ls} = \eta_e \left\{ \frac{E_1}{36} C_w^2 \frac{\bar{a}^2(1-\varepsilon)^2 \mu_l \eta_e}{\varepsilon_l^3} + \frac{E_2}{6}(1+\psi_{gl}) C_{wi} \frac{\bar{a}(1-\varepsilon)}{\varepsilon_l^3} \rho_l \left| v_l \right| \right\} v_l \varepsilon_l \quad (36)$$

$$F_{gs} = (1-\eta_e) \left\{ \frac{E_1}{36} C_w^2 \frac{\bar{a}^2(1-\varepsilon)^2 \mu_g}{\varepsilon^3} + \frac{E_2}{6} C_{wi} \frac{\bar{a}(1-\varepsilon)}{\varepsilon^3} \rho_g \left| v_g \right| \right\} v_g \varepsilon \quad (37)$$

$$F_{gl} = \eta_e \left\{ \frac{E_1}{36} C_w^2 \frac{\bar{a}^2(1-\varepsilon)^2 \mu_g}{(\varepsilon - \varepsilon_l/\eta_e)^2 \varepsilon_g} + \frac{E_2}{6} C_{wi}(1+\psi_{gl}) \frac{\bar{a}(1-\varepsilon)\rho_g}{(\varepsilon - \varepsilon_l/\eta_e)^2 \varepsilon_g} \left| v_g - (\varepsilon - \varepsilon_l/\eta_e) u^* \right| \right\} \times [v_g - (\varepsilon - \varepsilon_l/\eta_e) u^*] \varepsilon_g \quad (38)$$

Here v_l and v_g are the superficial velocities of the flowing phases based on the total cross-sectional area of the reactor, E_1 and E_2 are the bed Ergun viscous and inertial constants. Each one of the above drag force expressions involves a viscous contribution proportional to velocity and an inertial term expressed in a quadratic velocity dependency. To represent the gas–fluid relative motion intervening in F_{gl}, the effect of slip between the gas and liquid is accounted for by means of the velocity u^* at the gas–liquid interface derived in Iliuta et al.[49] and estimated from the double-slit model as

$$u^* = \frac{72}{E_1} \frac{\varepsilon_l}{(1-\varepsilon)^2 \bar{a}^2 \eta_e^2 \mu_l} \left[\frac{1}{2} \left(-\frac{\Delta P}{H} + \rho_l g \right) \varepsilon_l + \left(-\frac{\Delta P}{H} + \rho_g g \right) (\varepsilon \eta_e - \varepsilon_l) \right] \quad (39)$$

Effective specific surface area for liquid–solid momentum transfer

With the progress of fines deposition, the solid–liquid surface area is altered by two opposing phenomena[21]: an increase in surface area through addition of the area of the captured fine exposed to the stream line flow, and a loss of area A_Δ arising from the *shadow effect*[14] (the shadow effect refers to the fact that once a particle is captured by a collector certain parts of the collector surface near deposited particle are not accessible to approaching particles). The effective surface area can be expressed as the summation of the surface area of the porous medium and the surface area of the fines

$$\bar{a} = \frac{N_c \xi \pi d_p^2(t) + N_c \partial N_f [\xi \pi d_f^2 - A_\Delta(t)]}{N_c \dfrac{\pi}{6} (d_p^0)^3 + N_f \dfrac{\pi}{6} d_f^3} \quad (40)$$

The first term in the numerator of Eq. 40 reflects the area of the porous medium (that is, the collectors) and the second, the area of fines that becomes available for particle interception. Not all of the original media collector or the deposited fines is available for momentum transfer arising from packing structure, fracturing, or cul-de-sac formation. The geometrical parameter ξ, which represents the percentage of a single-particle surface area truly available for momentum transfer, has been included to account for this loss of area. According to the simulation results, about 55% of the surface area is available for momentum transfer and thus for particle capture. This

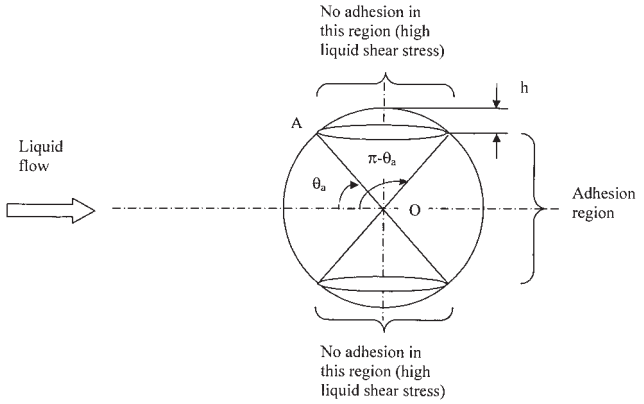

Figure 2. Portions of a collector where particle adhesion occurs.

value, which is in close agreement with previously recommended values proposed by Stephan and Chase[21] and Ortiz-Arroyo et al.,[22] states that particle collisions mostly exploit the upper frontal hemisphere of the collectors and the fines alike.

Fraction of the collector surface area available for the adhesion of fine particles

The fraction of the collector surface area available for the adhesion of fine particles corresponds to the regions where the shear stress acting on the collector is lower than the critical shear stress, respectively, $0 < \theta < \theta_a$ and $\pi - \theta_a < \theta < \pi$ (except north and south polar collector hemispheres; Figure 2)

$$\gamma = \frac{4\pi r_p^2 - 2 \times 2\pi r_p h}{4\pi r_p^2} \tag{41}$$

where

$$h = r_p - r_p \cos(90 - \theta_a) = r_p[1 - \sin \theta_a] \tag{42}$$

The final expression for the fraction of the collector surface area available for the fine particles adhesion is

$$\gamma = \sin \theta_a = \frac{\tau_{cr}}{\tau_{\pi/2}} \tag{43}$$

where the shear stress acting on the collector at $\theta = \pi/2$ was estimated using Happel's model (Eq. 31).

In the case of Brownian particles, the critical shear stress is very high and the entire particle surface area is available for particle adhesion. Therefore, Brownian particle release by hydrodynamic mechanism is precluded because of the far greater values of critical shear stress.

Method of Solution

To make the model (Eqs. 1–7) solvable, boundary and initial conditions need to be specified for the system in the trickle-flow regime. It is assumed that there is an inlet of gas and liquid at the top of the reactor and an outlet at its bottom. The pressure, the concentration of fine particles, the liquid and gas holdups, and the gas and liquid interstitial velocities are specified at the inlet. To solve the system of partial differential equations, we discretized in space and solved the resulting set of ordinary differential equations. The spatial discretization is performed using the standard cell-centered finite-difference scheme. The Gear integration method (also called backward differentiation) for stiff differential equations was used to integrate the time derivatives.

Transient flow simulations in a clean bed are first performed until the (pressure, velocity, and holdup) flow fields reach steady state. Under these circumstances, the conservation equations (Eqs. 8–12) are solved in the absence of fines in the liquid along with the effective specific surface area calculated using Eq. 40. Starting from these solutions, transient simulations with fines-containing liquid are then resumed by solving Eqs. 1–7. Simulations are carried out on a Pentium IV processor running at 2500 MHz. The relative error tolerance for the time-integration process in the present simulations is set at 10^{-5} for each time step.

Results and Discussion

Experimental verification

In a previous work, we validated a filtration model for two-phase flow coupled with a fines deposition process only.[3] However, there is no single work in the literature about two-phase flow in which coupling between deposition and release processes of fine particles in trickle-bed reactors has been attempted. Moreover, to the best of our knowledge, the concept of induced pulsing as a potential means for struggling against filtration in trickle beds has never been explored in the past. For both such reasons, no experimental data can be procured for validation of this new approach for conducting periodic filtration. Therefore, we will illustrate in this investigation the theoretical promises, if any, that this novel method could hold.

Estimation of model parameters

To make the model solvable, the Ergun constants (E_1 and E_2), the liquid axial dispersion coefficient (D_l), and the external wetting efficiency (η_e) need to be specified. The Ergun single-phase flow parameters can either be set by measurements of single-phase pressure drops[48] or estimated from literature correlations.[50] The wetting efficiency was evaluated using the comprehensive neural network correlation developed by Larachi et al.[51] The extent of back-mixing in the liquid phase is quantified in terms of an axial dispersion coefficient that is evaluated using a recent comprehensive Bodenstein number correlation.[52]

Simulation

Capture, release, and migration of fine particles in two-phase flow porous media systems are complex so that flow-field imaging of the transient phenomena accompanying fluid flow and both deposition and release of fine particles is not trivial and has not yet been experimentally attempted. It is proposed here to test the model potentiality through simulations of different experimental configurations by solving the transport equations for trickle-bed reactors experiencing deep-bed filtration. Plugging tests (room temperature) are run using kerosene as the liquid phase (seeded with kaolinite fine particles) and air

Table 1. Model Parameters

Property	Value
Liquid: Kerosene	
Viscosity	2 MPa · s
Density	801 kg/m^3
Surface tension	0.030 N/m
Gas: Air	
Density	1.3 kg/m^3
Fine particles: Kaolinite	
Average diameter	1–15 μm
Density	2000 kg/m^3
Porosity of deposit layer[38]	0.8
Influent concentration	0.1–1.0 g/L
Packing: Spherical catalyst particles	
Diameter	0.004 m
Bed porosity	0.385
Geometry of fixed-bed reactor	
Diameter	0.038 m
Height	1.0 m
Coefficient of sliding friction[32]	$k_f = 3.79 \times 10^{-6}$ m
Hamaker constant	Ha = 2.2×10^{-20} J

as the gas phase. Spherical (γ-alumina) catalytic particles are used as collectors. The simulated conditions are listed in Table 1 and coincide with typical hydrotreating conditions as discussed by Gray and co-workers.[2,5,24] To illustrate the quantitative and qualitative features of deposition and release of fine particles in a trickle-flow regime, the simulated results to follow are presented (1) in terms of longitudinal profile snapshots of the local porosity and specific deposit as well as (2) in the form of transient pressure drop buildup, at different liquid superficial velocities and fine particle diameters under liquid flow shear shock, or either periodic or normal operation conditions.

When a trickle-bed reactor, fed with heavy gas oil suspensions containing a low concentration of nonfilterable fine solid impurities, is operated under liquid flow shock or periodic operation conditions, release or inhibition of fine particles deposition in some regions of the collector can be expected after the liquid shear shock. Consequently, the model presented in this work is analyzed to gain better insight into the effect of liquid flow shock and periodic operation on trickle-bed deep-bed filtration. The purpose of this study is to analyze theoretically the release of fine particles in two-phase flow in a way similar to that investigated in the case of single-phase flow filtration under liquid flow shear shock by Bai and Tien.[32]

The first set of simulations concerns non-Brownian deposition/release (hydrodynamic release) of fine particles under periodic and normal operation conditions. In the periodic mode of operation, the liquid feed is cycled while the gas is continuously fed. Figure 3 presents a schematic illustration of the characterization of the cycled liquid feed (where v_{lb} is low liquid feed, v_{lp} is high liquid feed, t_b is the duration of low liquid feed, and t_p is the duration of high liquid feed).

Figures 4 and 5 show snapshots at $t = 833$ min of the longitudinal profiles of the specific deposit and the corresponding local porosity for two different liquid flow shear shocks in the case of non-Brownian fine particles. The figures reveal a noticeable decrease in local porosity in the entrance section of the catalyst bed that is coherent and also mirrored by the increased specific deposit. Periodic operation of the trickle bed reduces the specific solid deposit in the reactor. For a cycled

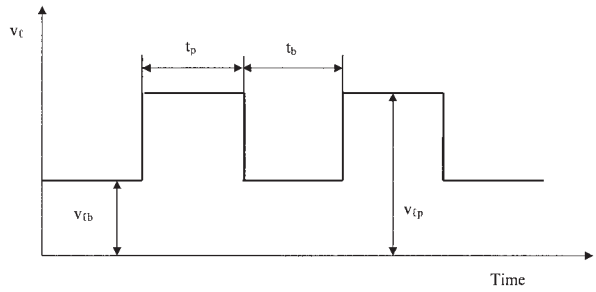

Figure 3. Schematic illustration of the characterization of the cycled liquid feed.

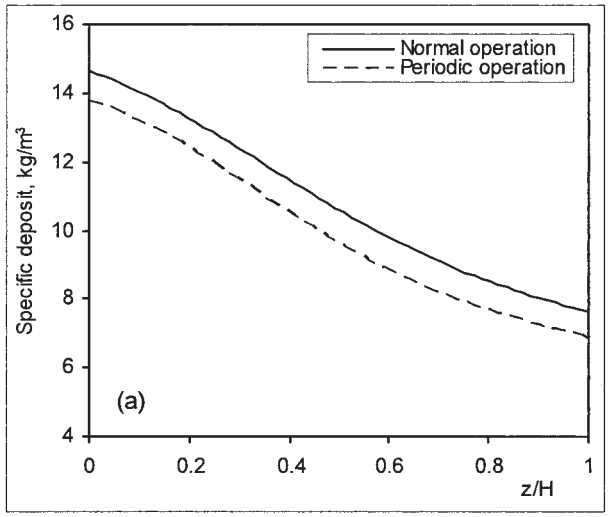

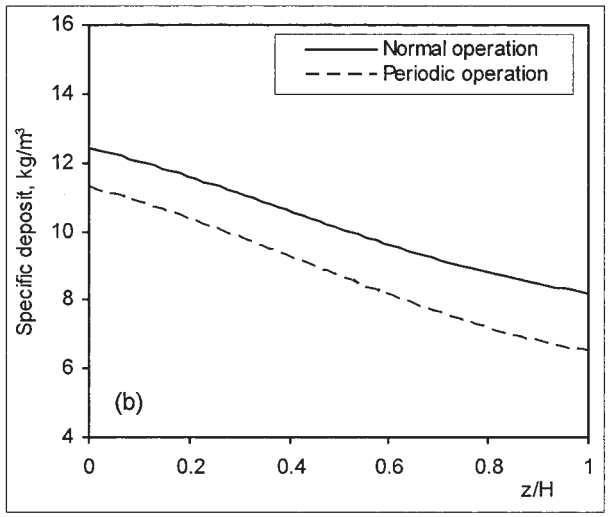

Figure 4. Variation of specific deposit with the dimensionless axial distance for normal (at an average superficial liquid velocity) and periodic operation.

$d_f = 15$ μm, $c_0 = 0.1$ g/L, $\alpha^h_{\text{det}} = 1.4 \times 10^{-8}$ kg N^{-1} s^{-1}. (a) periodic operation: $v_{lp} = 0.006$ m/s, $v_{lb} = 0.003$ m/s, $t_p = 500$ s, $t_b = 500$ s; normal operation: $v_l = 0.0045$ m/s; (b) periodic operation: $v_{lp} = 0.009$ m/s, $v_{lb} = 0.003$ m/s, $t_p = 500$ s, $t_b = 500$ s; normal operation: $v_l = 0.006$ m/s. $v_g = 0.1$ m/s in all cases.

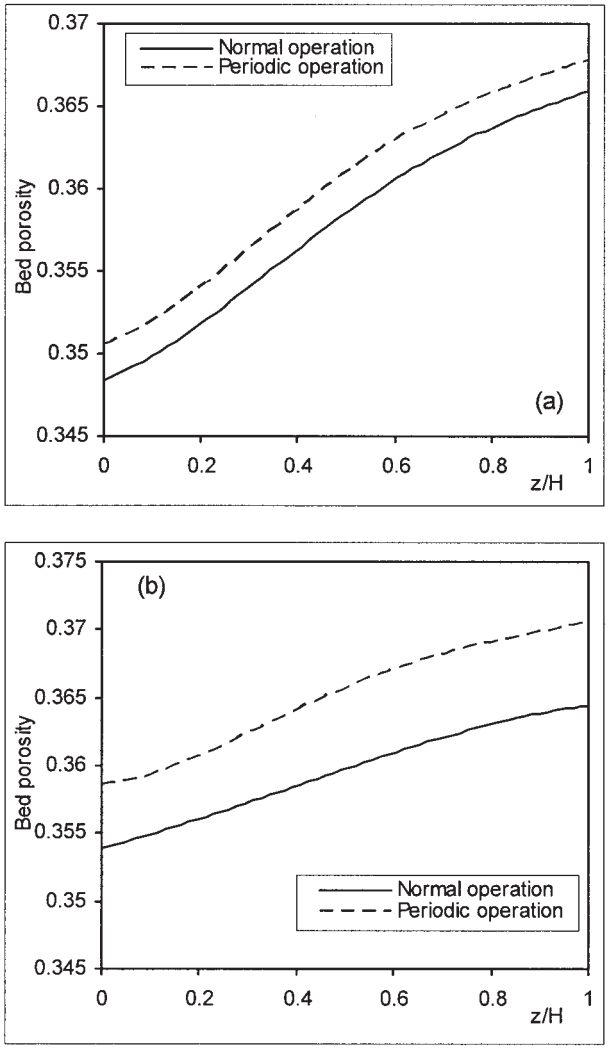

Figure 5. Variation of local bed porosity with the dimensionless axial distance for normal and periodic operation.

$d_f = 15\ \mu$m, $c_0 = 0.1$ g/L, $\alpha^h_{\text{det}} = 1.4 \times 10^{-8}$ kg N^{-1} s^{-1}: (a) periodic operation: $v_{lp} = 0.006$ m/s, $v_{lb} = 0.003$ m/s, $t_p = 500$ s, $t_b = 500$ s; normal operation: $v_l = 0.0045$ m/s; (b) periodic operation: $v_{lp} = 0.009$ m/s, $v_{lb} = 0.003$ m/s, $t_p = 500$ s, $t_b = 500$ s; normal operation: $v_l = 0.006$ m/s. $v_g = 0.1$ m/s in all cases.

liquid feed operation with $v_{lp} = 2v_{lb}$ and for a hydrodynamic release rate coefficient $\alpha^h_{\text{det}} = 1.4 \times 10^{-8}$ kg N^{-1} s^{-1} (Figure 4a), the average specific deposit decreases by 8.1% compared with that of the normal operation at $v_l = 0.0045$ m/s. Periodic operation of the reactor reduces the specific solid deposit because the fraction of the collector surface area available for the adhesion of fine particles (γ) decreases with the increase in liquid velocity and, on the other hand, because the hydrodynamic release of fine particles increases as a result of the increase of the wall shear stress. The decrease of specific solid deposit in the reactor is more significant at higher liquid flow shear shock (Figure 4b). Thus, for a cycled liquid feed operation with $v_{lp} = 3v_{lb}$ and for a hydrodynamic release rate coefficient $\alpha^h_{\text{det}} = 1.4 \times 10^{-8}$ kg N^{-1} s^{-1} (Figure 4b), the average specific deposit decreases by 14% compared with that of normal operation at $v_l = 0.006$ m/s.

When a liquid suspension passes through a bed, some of the fines are retained by the bed (the deposition being caused by diffusion, interception, gravitational collection, and collection attributed to surface forces) and two-phase pressure drop (ΔP) increases compared to that for the clean bed without fines (ΔP^0) (see Figures 6a and 6b). The major change resulting from deposition of fine particles involves bed porosity and therefore the increase of two-phase pressure drop is the result of a decrease in bed porosity. Figure 6 shows that two-phase pressure drop ratio is lower in the case of trickle-bed periodic operation as a result of lower values of specific deposit (respectively, larger values of local porosity). This evident decrease is more significant at higher liquid flow shear shock.

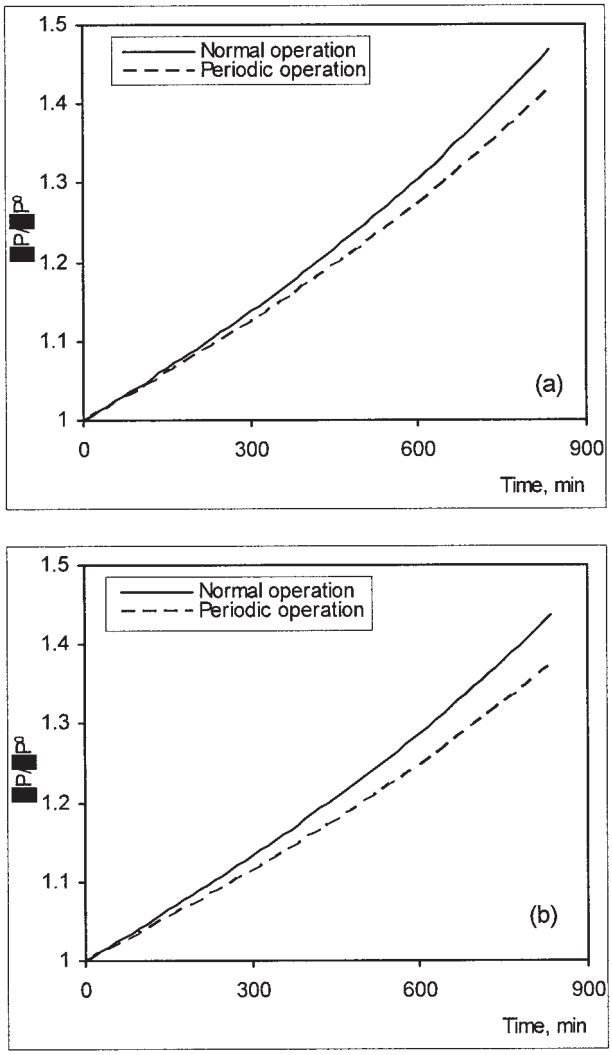

Figure 6. Impact of periodic operation on transient behavior of the two-phase pressure drop for normal and periodic operation.

$d_f = 15\ \mu$m, $c_0 = 0.1$ g/L, $\alpha^h_{\text{det}} = 1.4 \times 10^{-8}$ kg N^{-1} s^{-1}: (a) periodic operation: $v_{lp} = 0.006$ m/s, $v_{lb} = 0.003$ m/s, $t_p = 500$ s, $t_b = 500$ s; normal operation: $v_l = 0.0045$ m/s; (b) periodic operation: $v_{lp} = 0.009$ m/s, $v_{lb} = 0.003$ m/s, $t_p = 500$ s, $t_b = 500$ s; normal operation: $v_l = 0.006$ m/s. $v_g = 0.1$ m/s in all cases.

Note also that the saw-toothed pressure drop behavior expected from the induced pulsing programming is not visible in Figures 6a and 6b because of two main reasons: (1) the induced pulsing cycle period of about 15 min is negligibly small compared to the timescale of filtration (up to 900 min), and (2) the positive and negative peak pressure drop amplitudes are absorbed during normalization as a result of the high absolute value of ΔP^0.

Higher values of hydrodynamic release rate coefficient translate into a higher value of the rate of hydrodynamic particle entrainment, resulting in lower specific deposit for periodic operation (Figure 7). Under a cycled liquid feed operation with $v_{lp} = 2.4v_{lb}$ and for a hydrodynamic release rate coefficient $\alpha^h_{\text{det}} = 1.4 \times 10^{-8}$ kg N^{-1} s^{-1} (Figure 7a), the average specific deposit decreases by 11% compared with that of the normal operation at $v_l = 0.0051$ m/s. By increasing the hydrodynamic release rate coefficient at 80.0×10^{-8} kg N^{-1} s^{-1} (Figure 7b)

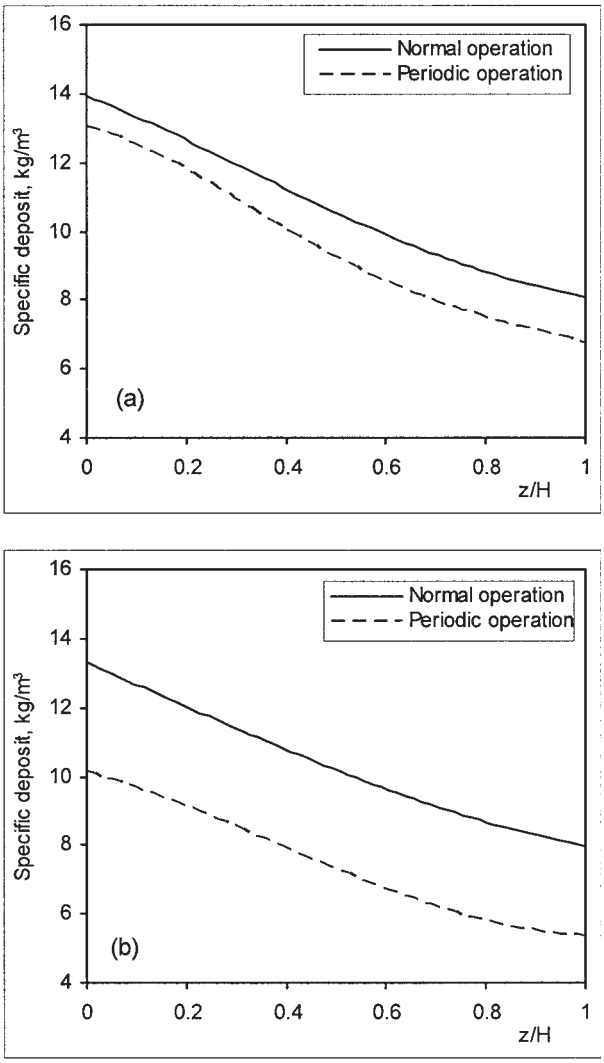

Figure 7. Impact of hydrodynamic release rate coefficient on the specific solid deposit for normal and periodic operation.

$d_f = 15$ μm; $c_0 = 0.1$ g/L; periodic operation: $v_{lp} = 0.0072$ m/s, $v_{lb} = 0.003$ m/s, $t_{p_h} = 500$ s, $t_b = 500$ s; normal operation: $v_l = 0.0051$ m/s. (a) $\alpha^h_{\text{det}} = 1.4 \times 10^{-8}$ kg N^{-1} s^{-1}; (b) $\alpha^h_{\text{det}} = 80.0 \times 10^{-8}$ kg N^{-1} s^{-1}; $v_g = 0.1$ m/s in all cases.

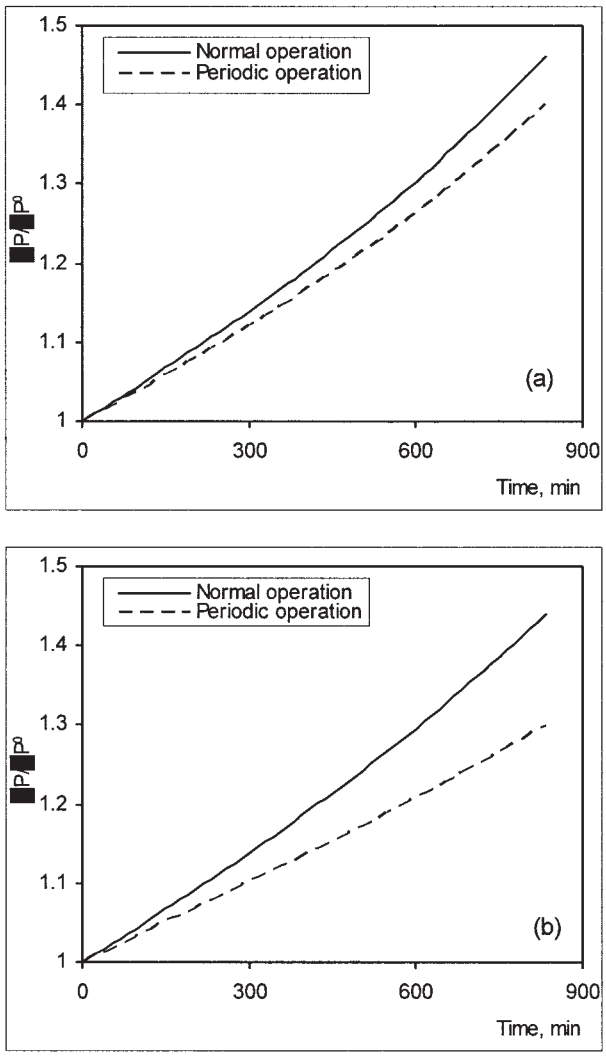

Figure 8. Impact of hydrodynamic release rate coefficient on the transient behavior of the two-phase pressure drop for normal and periodic operation.

$d_f = 15$ μm; $c_0 = 0.1$ g/L; periodic operation: $v_{lp} = 0.0072$ m/s, $v_{lb} = 0.003$ m/s, $t_{p_h} = 500$ s, $t_b = 500$ s; normal operation: $v_l = 0.0051$ m/s. (a) $\alpha^h_{\text{det}} = 1.4 \times 10^{-8}$ kg N^{-1} s^{-1}; (b) $\alpha^h_{\text{det}} = 80.0 \times 10^{-8}$ kg N^{-1} s^{-1}. $v_g = 0.1$ m/s in all cases.

the average specific deposit decreases by 28%. As a result, at a higher hydrodynamic release rate coefficient there is an evident decrease of two-phase pressure drop ratio in the reactor (Figure 8).

Release of fine particles was observed to be much more profound for larger fine particles than for smaller ones (Figure 9). For a cycled liquid feed operation with $v_{lp} = 3.0v_{lb}$ and for a hydrodynamic release rate coefficient $\alpha^h_{\text{det}} = 1.4 \times 10^{-8}$ kg N^{-1} s^{-1}, the average specific deposit decreases by 14 and 12.7% (for d_f values of 15 and 12 μm, respectively), compared with the normal operation at $v_l = 0.006$ m/s. By increasing the hydrodynamic release rate coefficient at 80.0×10^{-8} kg N^{-1} s^{-1} (Figure 9b), the average specific deposit decreases by 48.7 and 23.5% (for d_f values of 15 and 12 μm, respectively), compared with the normal operation. Also, the decrease of

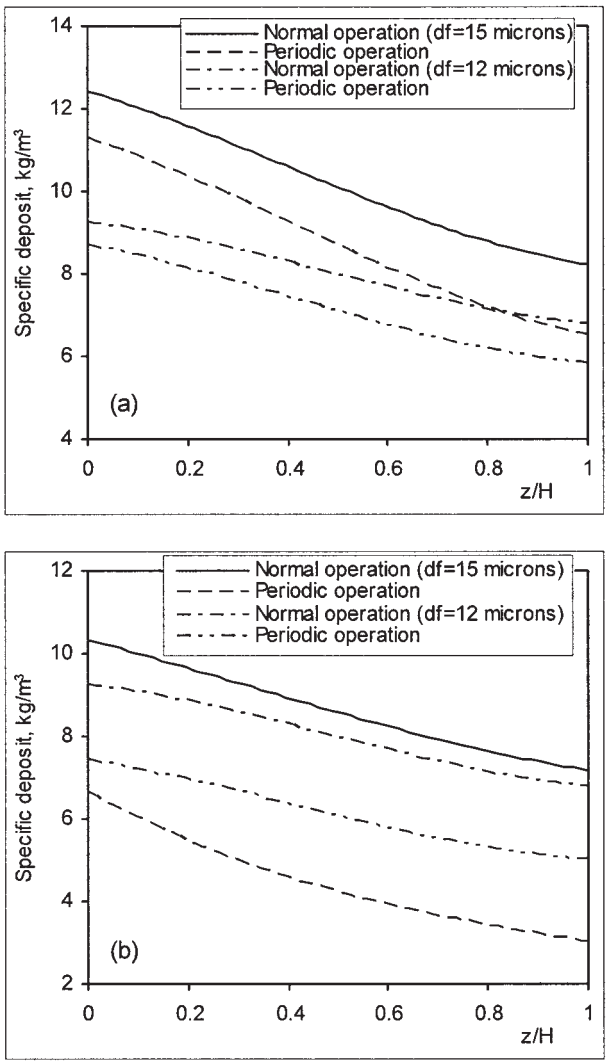

Figure 9. Variation of specific deposit with the dimensionless axial distance for normal and periodic operation.

$c_0 = 0.1$ g/L; periodic operation: $v_{lp} = 0.009$ m/s, $v_{lb} = 0.003$ m/s, $t_p = 500$ s, $t_b = 500$ s; normal operation: $v_l = 0.006$ m/s. (a) $\alpha^{fr}_{det} = 1.4 \times 10^{-8}$ kg N^{-1} s^{-1}; (b) $\alpha^{h}_{det} = 80.0 \times 10^{-8}$ kg N^{-1} s^{-1}. $v_g = 0.1$ m/s in all cases.

two-phase pressure drop ratio in the case of trickle-bed periodic operation is more significant for larger fine particles than for smaller ones (Figure 10).

The second set of simulations concerns non-Brownian deposition/release (hydrodynamic release) of fine particles under liquid flow shock conditions. So, the liquid flow rate through the trickle-bed reactor is sometimes suddenly increased. During the liquid flow shock, the feed concentration of fine particles was set to zero.

Figure 11 shows the evolution of volume-averaged specific deposit in time before and after the liquid flow shear shock. Before the liquid flow shear shock only deposition of fine particles occurs because the wall shear stress is lower than the critical shear stress. After the liquid flow shear shock only release of fine particles occurs because during the liquid flow shock ($t > 418$ min) the feed concentration of fine particles was set to zero and because the wall shear stress is larger than the critical shear stress. The detachment of fine particles was largely enhanced in the case of greater liquid flow shear shock. Figure 11 suggests that a large liquid flow shear shock can decongest the trickle-bed reactor after a time duration comparable to the deposition time duration.

The third set of simulations concerns the Brownian deposition/release (colloidal release) of fine particles under liquid flow shear shock or periodic operation conditions.

Periodic operation of the reactor reduces the specific solid deposit for the reason that colloidal fine particles release rate increases slowly with the increase of liquid flow velocity. However, this reduction is not substantial: under a cycled liquid feed operation with $v_{lp} = 3v_{lb}$ the average specific deposit decreases by only 3% compared with that of normal operation at $v_l = 0.006$ m/s. Therefore, periodic operation is

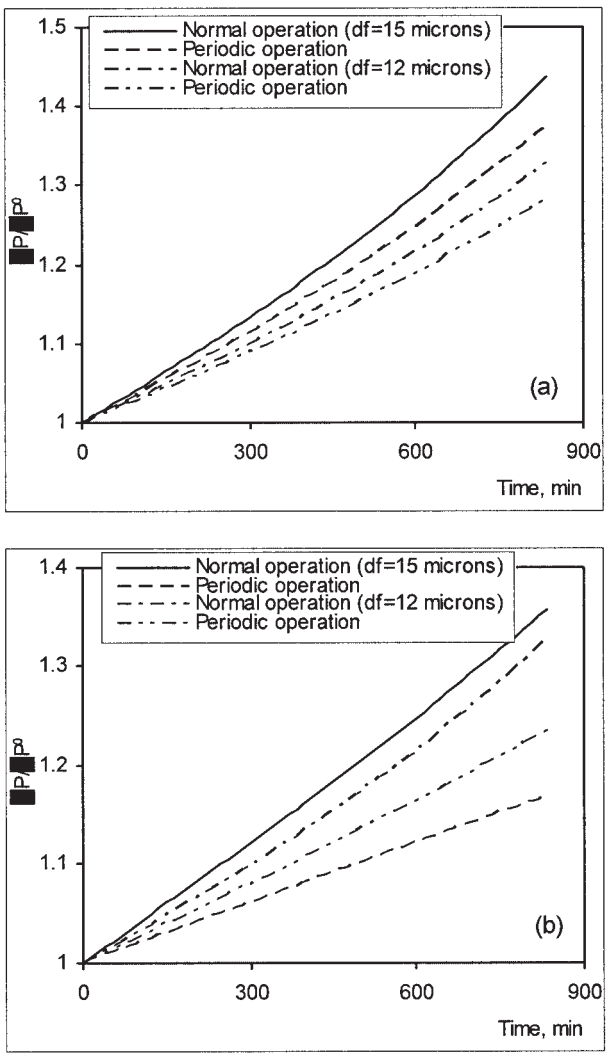

Figure 10. Two-phase pressure drop ratio vs. time at different values of fine particles diameter for normal and periodic operation.

$c_0 = 0.1$ g/L; periodic operation: $v_{lp} = 0.009$ m/s, $v_{lb} = 0.003$ m/s, $t_p = 500$ s, $t_b = 500$ s; normal operation: $v_l = 0.006$ m/s. (a) $\alpha^{h}_{det} = 1.4 \times 10^{-8}$ kg N^{-1} s^{-1}; (b) $\alpha^{h}_{det} = 80.0 \times 10^{-8}$ kg N^{-1} s^{-1}. $v_g = 0.1$ m/s in all cases.

not a viable solution for mitigation of plugging in trickle-bed reactors resulting from Brownian fine particles. In these circumstances, plugging inhibition may better be conducted under liquid flow shock conditions (replacing suspension flow with clean liquid flow at higher liquid flow rate) as will be seen next.

As in the case of non-Brownian fine particles, the simulations concerning the deposition/release (colloidal release) of Brownian fine particles under liquid flow shock conditions (Figure 12) show that before liquid flow shear shock deposition of fine particles occurs and after liquid flow shear shock only release of fine particles occurs. Similarly, during liquid flow shock ($t > 418$ min), the feed concentration of fine particles was reduced to zero (no particle adhesion). However, in the case of Brownian fine particles a longer period is needed to decongest the trickle-bed reactor.

Conclusion

A dynamic multiphase flow model, based on the volume-average mass and momentum balance equations and volume-average species balance equation for fine particles, was proposed for the description of two-phase flow, space–time evolution of both deposition and release of fine particles in trickle-bed reactors. The coupling between the fluid and solid phases was monitored by the fine particles filter equation, particle release rate equations, and the interaction drag or momentum exchange force terms. Both monolayer and multiple-layer deposition mechanisms were accounted for by including the appropriate filter coefficient formulation. The release of the fine particles from the collector surface was supposed to be induced by the colloidal forces in the case of Brownian particles or by the hydrodynamic forces in the case of non-Brownian particles. The impact of fine particles was analyzed in terms of longitudinal profile snapshots of the local porosity and specific deposit as well as in the form of transient pressure drop buildup, at different liquid superficial velocities and diameters of fine particles under liquid flow shear shock or either periodic or normal operation conditions. The following conclusions can be drawn from the simulation results:

- in the case of non-Brownian particles, periodic operation of the trickle bed reduces the specific solid deposit (and plugging) in the reactor;
- the release of fine particles was observed to be much more intense for larger fine particles than for smaller ones;
- the release of fine particles was largely enhanced in the case of larger liquid flow shear shock;
- periodic operation is not a viable solution for the attenuation of plugging in trickle-bed reactors attributed to Brownian fine particles.

The authors frankly recognize that this theoretical work is mainly illustrative of the potential of the filtration formalism that we extended to analyze a novel category of problems belonging to the realm of gas–liquid multiphase-flow petroleum refining problems. We hope the present effort will trigger future experimental studies to test the value of our model under induced pulsing conditions.

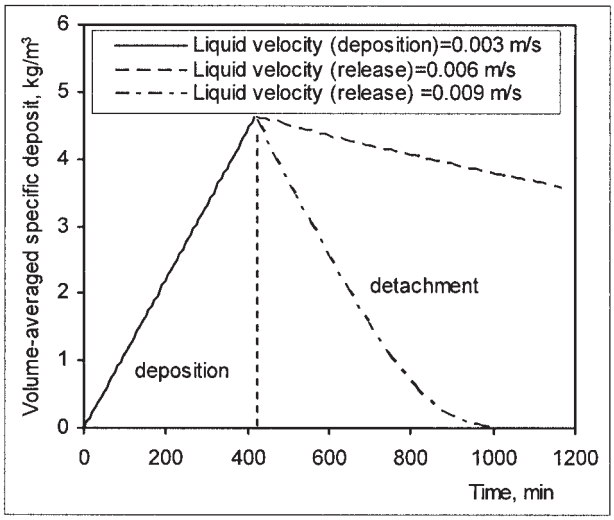

Figure 11. Variation of volume-averaged specific deposit in time before (c_0 = 0.1 g/L) and under liquid flow shear shock (c_0 = 0.0 g/L, α^{h}_{det} = 80.0 × 10^{-8} kg N^{-1} s^{-1}) for non-Brownian fine particles (d_f = 15 μm).

v_g = 0.1 m/s in all cases.

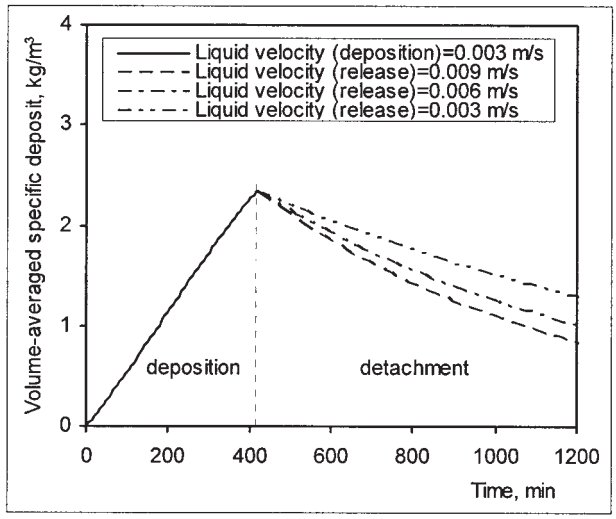

Figure 12. Variation of volume-averaged specific deposit in time before (c_0 = 1.0 g/L) and under liquid flow shear shock (c_0 = 0.0 g/L) for Brownian fine particles (d_f = 1 μm).

v_g = 0.1 m/s in all cases.

Acknowledgments

Financial support from the Natural Sciences and Engineering Research Council (NSERC) of Canada through its Strategic Program Grants is acknowledged.

Notation

$\bar{a}$ = effective specific surface area (surface of the particles/volume of the solid phase), m^2/m^3_s
a_s = specific area of the packing (surface of the particles/volume of the bed), m^2/m^3
A_Δ = collector area loss, $A_\Delta = (1/2)[d_p(t)/2]^2\langle\{2\sqrt{3}[d_f/d_p(t)]\} - \sin\{2\sqrt{3}[d_f/d_p(t)]\}\rangle$, m^2
c = fine volumetric concentration (liquid volume basis)
d_c = column diameter, m
d_f = fine particle diameter, m

d_p = effective particle diameter, $d_p(t) = d_p^0 \sqrt[3]{1 + \frac{\sigma}{(1-\varepsilon_d)(1-\varepsilon^0)}}$, m
D_{BM} = Brownian diffusion coefficient, $D_{BM} = 2k_BT/6\pi\mu_l d_f$
D_l = axial dispersion coefficient in liquid phase, m^2/s
E_1, $E2$ = Ergun constants
F_{gl} = gas–liquid drag force, N/m^3
F_{gs} = gas–solid drag force, N/m^3
F_{ls} = liquid–solid drag force, N/m^3
g = gravity acceleration, m/s^2
H = bed height, m
Ha = Hamaker constant, J
k_B = Boltzmann's constant, J/K
k_F = coefficient of sliding friction, m
k_L = coefficient for the lifting force
N = filtration rate (reactor volume basis), s^{-1}
N_c = number of collectors in grid cell volume v, $N_c = [6v/\pi(d_p^0)^3](1-\varepsilon^0)$
N_f = number of trapped fines in grid cell volume v, $N_f = (6v/\pi d_f^3)(\varepsilon^0 - \varepsilon)(1-\varepsilon_d)$
∂N_f = number of peripheral fines per collector, $\partial N_f = 4\beta(1-\varepsilon_d)[d_p(t)/d_f]^2$
N_G = gravitational dimensionless group, $N_G = [(\rho_f - \rho_l)d_f^2 g]/18\pi\mu_l v_l$
N_L = London–van der Waals dimensionless group, $N_L = 4Ha/9\pi\mu_L d_f^2 v_l$
N_{Pe} = Brownian diffusion group, $N_{Pe} = d_p(t)v_l/D_{BM}$
N_R = interception dimensionless group, $N_R = d_f/d_p^0$
P = pressure, Pa
R = constant of ideal gas, J kg^{-1} K^{-1}
T = temperature, K
t_b = duration of base feed, s
t_p = duration of pulse feed, s
u_α = average interstitial velocity of α-phase, m/s
v = grid cell volume, m^3
v_α = α-phase superficial velocity, m/s
v_{lp} = liquid superficial velocity during high liquid feed, m/s
v_{lb} = liquid superficial velocity during low liquid feed, m/s

Greek letters

α_{det}^c = colloidal first-order release rate coefficient, s^{-1}
α_{det}^h = hydrodynamic release rate coefficient, kg N^{-1} s^{-1}
β = collector cross-section fraction, $\beta = 1 - \frac{1}{2}\left[\frac{d_p^0}{d_p(t)}\right]^2\left[1 - \frac{d_p(t)}{d_p(t)+2d_f}\right]$
ε = bed porosity
$\langle\varepsilon\rangle$ = bed volume-averaged porosity
ε_d = porosity of deposits
ε_g = gas holdup
ε_l = liquid holdup
δ_{bl} = thickness of the boundary layer around a single spherical colloid, $\delta_{bl} = r_p(D_{BM}/u_l r_p)^{1/3}$
γ = fraction of the collector surface area available for the adhesion of fine particles
η = collector efficiency
η_e = wetting efficiency
λ = filter coefficient, m^{-1}
λ_0 = clean filter coefficient, m^{-1}
μ_α = α-phase dynamic viscosity, kg m^{-1} s^{-1}
μ_α^e = α-phase effective viscosity (combination of bulk and shear terms), kg m^{-1} s^{-1}
ρ_α = density of α-phase, kg/m^3
σ = specific deposit (reactor volume basis), $\sigma = (\varepsilon^0 - \varepsilon)(1-\varepsilon_d)$
$\langle\sigma\rangle$ = bed volume-averaged specific deposit, $\langle\sigma\rangle = H^{-1}\int_0^H \sigma(t)dz$
σ_l = surface tension, N/m
τ = shear stress on the collector plan, N/m^2
ξ = surface-area parameter
ψ_{gl} = gas–liquid interaction factor

Subscripts

f = fine
g = gas phase
l = liquid phase
s = solid phase

Superscript

0 = clean bed state (initial)

Literature Cited

1. Narayan R, Coury JR, Masliyah JH, Gray MR. Particle capture and plugging in packed-beds reactors. *Ind Eng Chem Res.* 1997;36:4620-4627.
2. Gray MR, Srinivasan N, Masliyah JH. Pressure buildup in gas–liquid flow through packed beds due to deposition of fine particles. *Can J Chem Eng.* 2002;80:346-354.
3. Iliuta I, Larachi F, Grandjean BPA. Fines deposition dynamics in trickle flow reactors. *AIChE J.* 2003;49:485-495.
4. Iliuta I, Larachi F. Fines deposition dynamics in packed-bed bubble reactors. *Ind Eng Chem Res.* 2003;42:2441-2449.
5. Wang S, Chung KH, Masliyah JH, Gray MR. Deposition of fine particles in packed beds at hydrotreating conditions: Role of surface chemistry. *Ind Eng Chem Res.* 1999;38:4878-4888.
6. Herzig JP, Leclerc DM, Le Goff P. Flow of suspensions through porous media. Application to deep bed filtration. *Ind Eng Chem.* 1970;62:8-35.
7. Yao KM, Habibian MT, O'Melia CR. Water and waste water filtration: Concepts and applications. *Environ Sci Technol.* 1971;5:1105-1112.
8. Spielman LA, Fitzpatrick JA. Theory of particle collection under London and gravity forces. *J Colloid Interface Sci.* 1973;42:607-623.
9. Payatakes AC, Tien C, Turian RM. Trajectory calculation of particle deposition in deep bed filtration—Part I. *AIChE J.* 1974a;20:889-899.
10. Payatakes AC, Tien C, Turian RM. Trajectory calculation of particle deposition in deep bed filtration—Part II. *AIChE J.* 1974b;20:900-905.
11. Rajagopalan R, Tien C. Trajectory analysis of deep-bed filtration with the sphere-in-cell porous media model. *AIChE J.* 1976;22:523-533.
12. Rajagopalan R, Tien C. Single collector analysis of collection mechanisms in water filtration. *Can J Chem Eng.* 1977;55:246-255.
13. O'Melia CR, Ali W. The role of retained particles in deep bed filtration. *Prog Water Technol.* 1987;10:167-175.
14. Tien C, Payatakes AC. Advances in deep bed filtration. *AIChE J.* 1979;25:737-759.
15. Pendse H, Tien C. A simulation model of aerosol collection in granular media. *J Colloid Interface Sci.* 1982;81:225-241.
16. Chiang HW, Tien C. Dynamics of deep bed filtration—Part I. Analysis of two-limiting situations. *AIChE J.* 1985;31:1349-1359.
17. Vigneswaran S, Tien C. Transient behavior of deep-bed filtration of Brownian particles. *Chem Eng Sci.* 1987;42:2729-2739.
18. Vigneswaran S, Tulachan RV. Mathematical modeling of transient behaviour of deep bed filtration. *Water Res.* 1988;22:1093-2001.
19. Choo CU, Tien C. Analysis of the transient behavior of deep-bed filtration. *J Colloid Interface Sci.* 1995a;169:13-33.
20. Cushing RS, Lawler DF. Depth filtration: Fundamental investigation through three-dimensional trajectory analysis. *Environ Sci Technol.* 1998;32:3793-3801.
21. Stephan EA, Chase GG. Development of volume-average theory for deep-bed filtration. *AIChE J.* 2000;46:1918-1926.
22. Ortiz-Arroyo A, Larachi F, Grandjean BPA, Roy S. Modeling and simulation of clogging in packed-bed reactors with non-aqueous media using CFD. *AIChE J.* 2002;48:1596-1609.
23. Chan EW, Chung KH, Veljkovic M, Liu JK. Hydrodynamics and fines capture in packed-bed hydrotreaters. Proc of Int Petrol Petrochem Technol Symp, Beijing, September 15–17; 1995.
24. Wang S, Chung KH, Gray MR. Role of hydrotreating products in deposition of fine particles in reactors. *Fuel.* 2001;80:1079-1085.
25. Iliuta I, Larachi F. Onset of pulsing in gas–liquid trickle bed filtration. *Chem Eng Sci.* 2004;59:1199-1211.
26. Ortiz-Arroyo A, Larachi F. Lagrange–Euler–Euler CFD approach for modeling deep bed filtration in trickle flow reactors. *Sep Purif Technol.* 2005;41:155-172.
27. Khilar KC, Fogler HS. *Migration of Fines in Porous Media*. Dordrecht, The Netherlands: Kluwer Academic; 1998.
28. Arulanandan K, Longanathan P, Krone KB. Pore and eroding fluid influences on surface erosion of soil. *J Geotech Eng Div ASCE.* 1975;101:51-65.
29. Khilar KC, Fogler HS. The existence of a critical salt concentration for particle release. *J Colloid Interface Sci.* 1984;100:214-224.

30. Ginn T, Amirtharajah A, Karr PR. Effects of particle detachment in granular-media filtration. *J Am Water Works Assoc*. 1992;84:66-76.
31. Moran MC, Moran DC, Cushing RS, Lawler DF. Particle behavior in deep-bed filtration: Part 2—Particle detachment. *J Am Water Works Assoc*. 1993;85:82-90.
32. Bai R, Tien C. Particle detachment in deep bed filtration. *J Colloid Interface Sci.* 1997;186:307-317.
33. Gruesbeck C, Collins RE. Entrainment and deposition of fines particles in porous media. *Soc Pet Eng J.* 1982;22:847-856.
34. Ryan JN, Gschwend PM. Effects of ionic strength and flow rate on colloid release: Relating kinetics to intersurface potential energy. *J Colloid Interface Sci.* 1994;164:21-34.
35. Khilar KC, Fogler HS. Water sensitivity of sandstones. *Soc Pet Eng J.* 1983;23:55-64.
36. Sharma MM, Yortsos YC. Transport of particulate suspensions in porous media: Model formulation. *AIChE J.* 1987;33:1636-1643.
37. Sen TK, Nalwaya N, Khilar KC. Colloid-associated contaminant transport in porous media: 2. Mathematical modeling. *AIChE J.* 2002;48: 2375-2385.
38. Tien C. *Granular Filtration of Aerosols and Hydrosols*. Stoneham, MA: Butterworths; 1989.
39. Choo CU, Tien C. Simulation of hydrosol deposition in granular media. *AIChE J.* 1995b;41:1426-1433.
40. Whitaker S. The transport equations for multi-phase systems. *Chem Eng Sci.* 1973;28:139-147.
41. Dankworth DC, Kevrekidis IG, Sundaresan S. Dynamics of pulsing in trickle beds. *AIChE J.* 1990;36:605-621.
42. Iwasaki T. Some notes on sand filtration. *J Am Water Works Assoc*. 1937;29:1591-1602.
43. Tien C, Turian RM, Pendse H. Simulation of the dynamic behavior of deep bed filters. *AIChE J.* 1979;25:385-404.
44. Burdick GM, Berman NS, Beaudoin SP. Describing hydrodynamic particle removal from surfaces using the particle Reynolds number. *J Nanoparticle Res.* 2001;3:455-467.
45. Israelachvili JN. *Intermolecular and Surface Forces*. 2nd Edition. London: Academic Press; 1991.
46. Goldman AJ, Cox RG, Brenner H. Slow viscous motion of a sphere parallel to a plane wall—II. Couette flow. *Chem Eng Sci.* 1967;22: 653-660.
47. Iliuta I, Larachi F, Al-Dahhan MH, Double-slit model for partially wetted trickle flow hydrodynamics. *AIChE J.* 2000;46:597-609.
48. Holub RA, Dudukovic MP, Ramachandran PA. A phenomenological model of pressure drop, liquid holdup and flow regime transition in gas–liquid trickle flow. *Chem Eng Sci.* 1992;47:2343-2348.
49. Iliuta I, Grandjean BPA, Larachi F. New mechanistic film model for pressure drop and liquid holdup in trickle flow reactors. *Chem Eng Sci*. 2002;57:3359-3371.
50. Iliuta I, Larachi F, Grandjean BPA. Pressure drop and liquid hold-up in trickle flow reactors: Improved Ergun constants and slip correlations for the slit model. *Ind Eng Chem Res*. 1998;37:4542-4550.
51. Larachi F, Belfares L, Grandjean BPA, Prediction of liquid–solid wetting efficiency in trickle flow reactors. *Int Commun Heat Mass Transfer*. 2001;28:595-603.
52. Piché S, Larachi F, Iliuta I, Grandjean BPA. Improving predictions of liquid back-mixing in trickle-bed reactors using a neural network approach. *J Chem Technol Biotechnol*. 2002;77:989-999.

Manuscript received Jun. 28, 2004, and revision received Nov. 23, 2004.